J Appl Electrochem (2016) 46:995–1010
DOI 10.1007/s10800-016-0978-5

RESEARCH ARTICLE

Methanol electro-oxidation on nanoporous metals formed by dealloying of Ag–Au–Pt alloys

Adrián A. Vega[1] · **Roger C. Newman**[1]

Received: 3 January 2016 / Accepted: 3 June 2016 / Published online: 20 June 2016

Abstract Novel nanoporous structures, with narrow distribution of pore and ligament sizes, were formed by electrochemical dealloying of ternary precursors (Ag–Au–Pt with platinum content of 1, 2, and 3 at.% and 77 at% of silver). These three-dimensional bicontinuous porous network structures proved to be active electrocatalysts for the methanol oxidation reaction. By changing the processing conditions (e.g., dealloying temperature) and/or post-dealloying treatments (e.g., exposure to moderately high temperature in the presence of air) of these structures, the characteristics of the resulting materials were modified (e.g., ligament size and platinum content on the surface of the ligaments) and with that their catalytic response. It was demonstrated that these high surface area nanostructures displayed enhanced specific activity and distinct surface reactivity compared with nanoporous gold formed by dealloying of Ag–Au alloy. Scanning electron microscopy, transmission electron microscopy, and electrochemical methods such as underpotential deposition of hydrogen and cyclic voltammetry were used to characterize the resulting nanoporous structures.

✉ Roger C. Newman
roger.newman@utoronto.ca

[1] Department of Chemical Engineering and Applied Chemistry, University of Toronto, 200 College Street, Toronto, ON M5S 3E5, Canada

Graphical Abstract

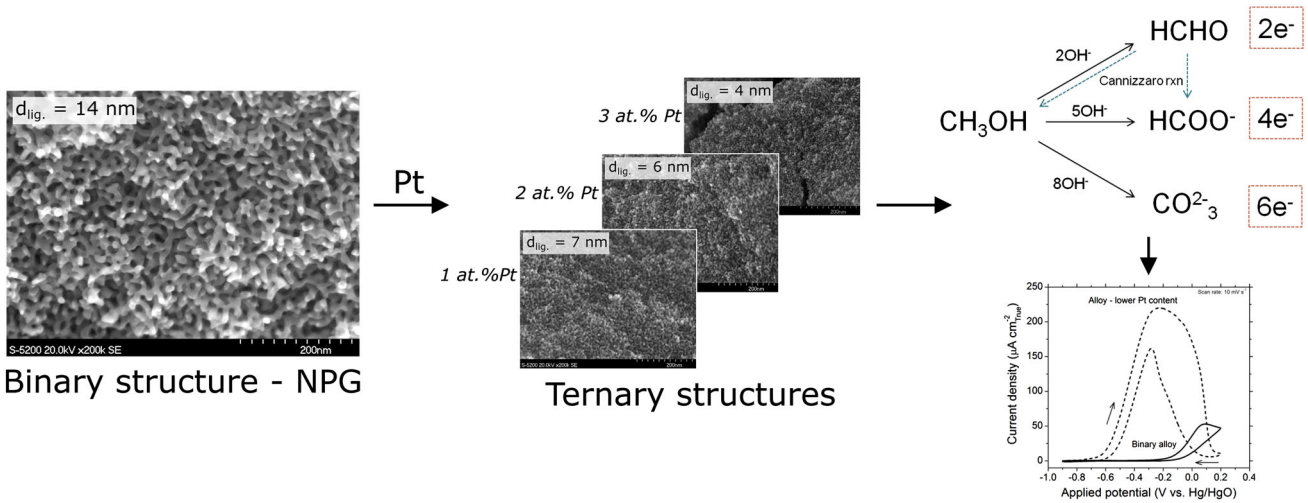

Keywords Dealloying · Electrocatalysis · Methanol oxidation reaction

1 Introduction

For centuries, gold has been recognized not only for its beauty and rarity, but also for its nobleness and inability to corrode. Historically, gold is an element that has been considered as a poor catalyst toward many technologically important reactions such as methanol electro-oxidation or carbon monoxide (CO) oxidation; however, it was recently observed that when this element is subdivided down to the nanoscale, it becomes a very reactive material [1–3]. Thus, the rapid development of nanotechnology and nanoscience has stimulated the application of gold in disciplines such as sensing and catalysis. Some of the reactions that have been catalyzed by nano-sized gold are low temperature CO oxidation [1], selective oxidation of benzyl alcohol [4, 5], the water gas shift reaction [2, 6], and many other reactions; some of which have been summarized elsewhere [7–9]. Among the different alternatives to study gold as a catalyst, gold nanoparticles have been commonly used. These nanoparticles, typically on a support, show a superior chemical stability, which enables them to act as a superior material for catalysis; however, small particles may suffer from shape stability issues and sintering over time, which reduces their active surface area and limits their long-term functionality [10–12]. Additionally, their processing usually involves relatively complicated preparation and assembly procedures [13–15]. Moreover, in supported gold catalysts, many factors have been correlated with the catalytic activity, including preparation methods of the catalyst, nature of the support, pre-treatment conditions, presence of water, and others [15–17].

Another alternative to produce nano-sized gold is to dealloy Ag–Au alloys to form nanoporous gold (NPG). By selectively leaching the silver from the Ag–Au alloy, highly porous nanostructures are formed, in which the interconnected interstices and channels extend in three dimensions. NPG has a desirable structure for catalysis, not only because of its high surface area, but also because it does not require a support. Moreover, it has been reported that the remarkable catalytic properties of NPG, which are also applicable to gold nanoparticles, are related to the high density of atomic steps and kinks (i.e., active sites) on the surface of the ligaments [18]. It has also been suggested that the residual silver in NPG played a significant role in its catalytic abilities, not only helping for adsorption/dissociation of molecules during chemical/electrochemical reactions, but also stabilizing the surface steps and kinks [18–20]. Furthermore, NPG is relatively easy to produce and its feature size is tunable from a few to hundreds of nanometers by post-heat treatment; unfortunately, NPG is prone to coarsening, reducing its functionality due to loss of surface area [21]. It has been shown that the microscopic surface diffusion of gold along the alloy/electrolyte interface is not only responsible for porosity evolution during dealloying, but also for the post-fabrication coarsening of the structure [22]. To minimize this coarsening, small amounts of platinum can be deposited onto the NPG film, with the resulting material having better stability even at high temperature conditions [21, 23–25]; however, this technique is time consuming and represents an extra step during the catalyst preparation process. Another alternative is to add platinum to the precursor material, as shown by Snyder et al. [26], after adding approximately 6 at% of platinum to the 'white-gold' type of Ag–Au alloy (i.e., gold content of 35 at%). We recently showed that with

the addition of as little as 1 at% of platinum to the alloy precursor, the coarsening of the structure is significantly minimized if compared with an alloy precursor with only gold [27]. In addition to the beneficial effect of platinum toward the stabilization of the nanostructure, it is expected that the presence of platinum and gold on the surface of the nanostructure will offer unique catalytic properties thanks to the synergy between these two elements [28–35]. It is believed that the strong chemisorption of oxygen species onto the porous gold will provide many reactive oxygenated species that may promote further oxidation of carbonaceous intermediates absorbed on the platinum surface; thus, the well-known poisoning effect on platinum-based catalysts will be reduced [36].

In this article, the electrocatalytic abilities of dealloyed multi-component alloy systems are reported. Specifically, alloys of Ag–Au–Pt have been selected with the same noble metal content and with a maximum platinum concentration of 3 at%. By selectively removing some of the silver from the ternary alloys, porous nanostructures were formed with well-controlled length scales and morphologies. The effect of nanoporous structures with a platinum-enriched surface, obtained by an *adsorbate-induced surface segregation* mechanism, is investigated; additionally, as another example of the tunability and flexibility of these structures, the effect on the catalytic response of structures formed at different dealloying temperatures is evaluated. Methanol electro-oxidation in basic medium was selected as our target system; however, some preliminary data of methanol oxidation in acidic media are also shown. NPG, formed by dealloying of Ag–Au alloy (with the same silver content as the ternary systems) is used as a control material. Most of the results included here were obtained from cyclic voltammetry in different reaction media, as well as scanning electron microscopy and transmission electron microscopy.

2 Experimental procedures

2.1 Alloys and dealloying procedures

Ag–Au alloy with 77 at% silver was obtained as cold-rolled 200 μm sheet from Goodfellow Metals, Cambridge, UK. Ag–Au–Pt alloys with platinum content of 1, 2, and 3 at% and 77 at% silver were obtained as cold-rolled sheet from Ames National Laboratory—US Department of Energy, Iowa, USA. For all the experiments, specimens were cut into strips of approximately 4 mm by 10 mm before annealing at 900 °C for 5 h in the case of the binary alloy and at 975 °C for 15 h in the case of the ternary alloys. In all cases, the annealing was performed in H_2–Ar atmosphere (2.5 % H_2; balance Ar). All the specimens were used in the as-annealed condition without any further surface preparation. Each strip of alloy was attached to a copper wire for electrical connection, using lacquer (SPI Miccroshield) to mask the junction and the isolated copper wire. In all cases, dealloying was done from both sides of the sample.

Dealloying was carried out potentiostatically in a three-electrode electrochemical cell (approximate volume 500 mL), with platinum coil as the counter electrode (CE) and mercury/mercurous sulfate (MSE, 0.64 V vs. SHE) as the reference electrode (RE). The RE electrode was housed in a separate compartment and connected to the electrochemical cell via a Luggin probe. In all cases, 0.77 M $HClO_4$ solution, prepared from Analar grade $HClO_4$ (Alfa-Aesar, 62 %), was used for dealloying. All solutions were prepared with 18 MΩ cm de-ionized water and de-aerated by high-purity nitrogen purging (min purity: 99.998 %). The electrochemistry was performed using a Gamry Reference 600^{TM} potentiostat. Most of the specimens were dealloyed at 25 °C, passing an anodic charge density of 5 C cm^{-2} at 0.55 V versus MSE; however, to study the effect of dealloying temperature, temperatures between 25 and 60 °C were evaluated (for the same charge density passed).

For some selected samples, the fraction of platinum exposed on the surface of the ligaments was tuned by the *adsorbate-induced surface segregation* phenomenon at 425 °C in laboratory air. For that purpose, the connecting wire was removed immediately after dealloying, and the specimens were thoroughly rinsed with de-ionized water and dried with air before exposed them to the target temperature. This phenomenon has been recently reported by the authors [37].

2.2 Characterization of the nanoporous structures

A detailed description of the characterization of these nanoporous structures has been given previously [27]. In summary, for the microstructural characterization (e.g., ligament size), dealloyed samples were manually broken under tension in air, and the fracture surface was photographed using a scanning electron microscope (SEM—Hitachi S-5200) with an accelerating voltage of 20 kV. The SEM pictures were later analyzed with the *Image Tool* software (provided by The University of Texas Health Science Centre in San Antonio, USA) to accurately determine the ligament size (here equivalent to the average width perpendicular to the ligament edge). The thickness of the dealloyed layer (DL) was determined after analyzing cross-sectional metallographic specimens.

In all cases, specimens were polished to 0.05 μm using alumina powder. The cross-sectional view of those specimens was photographed using an Olympus PME3 Optical Microscope and the DL thickness was measured using Clemex Vision Professional software. The composition of the DL was determined by SEM (JEOL JSM6610-Lv) complemented by an Oxford INCA X-sight energy-dispersive X-ray spectrometer (EDS) and by a transmission electron microscope (TEM—Hitachi HD-2000) complemented also by an Oxford INCA X-sight EDS. In the case of the TEM, selected samples were embedded in low viscosity resin (SPI-PON 812) and ultramicrotomed to 30–50 nm thickness using the Leica UltraCut R instrument equipped with a diamond knife. Accelerating voltages of 25 kV and 200 kV were used in the case of the SEM and TEM, respectively.

To evaluate the true surface area of the dealloyed specimens and the fraction of surface platinum atoms on the surface of the structure, classical electrochemical methods were used. The true area of the electrodes was estimated by means of voltammetric profiles in the double layer region of potentials (i.e., −0.24 to 0.05 V vs. MSE) at different scan rates in 1 M $HClO_4$ solution [38, 39]. In all cases, 28 μF cm^{-2} was considered the baseline double-layer capacitance for polycrystalline gold and platinum [38]. This assumption proved to be valid after comparing the results with Brunauer–Emmett–Teller (BET—Autosorb-1 Analyzer/Quantachrome Instruments) surface area and impedance measurements [27]. The pore size distribution of the resulting nanostructures was also obtained by the BET method. The equivalent area of platinum on the surface of the ligaments was estimated by underpotential deposition (UPD) of hydrogen [40, 41]. All specimens were immersed in 1 M H_2SO_4 solution (EMD, 95–98 %) in a three-electrode cell with a MSE as a RE, a platinum wire as CE, and the dealloyed specimen as a working electrode. The solution was de-aerated for approximately 15 min before the experiment. Cyclic voltammetry (CV) curves were obtained at 25 °C between −0.63 and 0 V versus MSE, at a scan rate of 20 mV s^{-1}. The equivalent area of platinum on the surface of the structure was calculated by integrating the hydrogen adsorption/desorption regions to obtain the charge related with the formation of a hydrogen monolayer, assuming that the charge associated with the monolayer formation in polycrystalline platinum was 210 μC cm^{-2} Pt [42, 43]. The fraction of platinum on the surface of the resulting structure was estimated by dividing the equivalent area of exposed platinum by the estimated true area of the electrode. The roughness factor (R_f), as an indication of the developed surface area during the dealloying process, was determined by dividing the true area of the electrode by its geometrical area.

2.3 Electro-oxidation of methanol

In the case of the electrocatalytic studies in basic media, dealloyed specimens were immersed in a solution containing methanol (Caledon, 99.8 %) in 5 M KOH (Aldrich, 90 %). Methanol concentrations of 0.3, 1, and 3 M were used for the analysis. The KOH/CH_3OH solution was prepared by diluting/dissolving the reactants with de-ionized water with a resistivity of 18 MΩ cm. Prior to any measurement, the solution was de-aerated by high-purity nitrogen purging (min purity: 99.998 %). A Gamry Reference 600^{TM} potentiostat was used to perform CV between −0.9 and 0.2 V versus mercury/mercury oxide RE (Hg/HgO—20 % KOH, 0.1 V vs. SHE). The effect of the positive scan limit was evaluated by changing it from 0 to 0.4 V versus Hg/HgO. Scan rates of 3, 10, 30, and 100 mV s^{-1} were used. To assess qualitatively the presence of any mass transfer effects during reaction, a magnetic stirrer was used. The approximate rotation velocity of the stirrer was measured with a digital laser tachometer (Fieldpiece, HP2234C). All current densities were normalized by the true area of the electrodes unless otherwise stated. Polycrystalline platinum was used as control material.

Additionally, potentiostatic experiments at −0.35/−0.40 V versus Hg/HgO (in the case of the ternary alloys) and at 0.05 V versus Hg/HgO (for the binary alloy) were carried out for 4000 s in the 5 M KOH–1 M CH_3OH solution. During these experiments, the solution was agitated with a magnetic stirrer with an approximated rotation velocity of 700 rpm. An evaluation of the products obtained as a result of the oxidation was done. The formation of formate was evaluated by nuclear magnetic resonance spectroscopy (H-NMR—Agilent DD2 500 MHz). For this analysis, 50 μL of solution was diluted in 5 mL of deuterium oxide (D_2O—Cambridge Isotope Laboratories, 99.9 %). Samples were then run using a scan at 90° pulse (16.1 μs) and 10 s relaxation delay, with an acquisition time of 4.5 s and spectral window of 8012 Hz. Standards with different formate contents were prepared for calibration purposes. The quantification of carbonate was done by titrating 5 mL of the resulting solution with 1.2 M $BaCl_2$ solution (ACP, 99 %). The $BaCl_2$ solution was prepared by dissolving the salt with de-ionized water with a resistivity of 18 MΩ cm. To avoid the precipitation of $Ba(OH)_2$, the pH was brought down from ca. 15.0 to ca. 10.0 by adding 2 mL of concentrated HCl (BioShop, 36.5–38 %) and a few drops of 2 M HCl solution. The HCl was added as quickly as possible to minimize the unnecessary exposure of the solution to air. Right after that, a solution of $BaCl_2$ was added drop wise while the pH was kept between 10.0 and 10.5 to avoid the dissolution of $BaCO_3$, which occurs at pH values around 6 [44–46]. Filtration of the obtained precipitate was done using a 0.45 μm membrane filter (PALL) followed by a gravimetric

determination. The contribution to the carbonate content from original slight carbonation of the KOH was measured by titrating the solution prior to the reaction.

For the electrocatalytic experiments in acidic media, selected specimens were immersed in a solution of 0.5 M $HClO_4$ (Alfa-Aesar, 60–62 %) and 1 M methanol (Caledon, 99.8 %). The $HClO_4/CH_3OH$ solution was prepared by diluting the reactants with de-ionized water with a resistivity of 18 MΩ cm. Prior to any measurement, the solution was de-aerated by high-purity nitrogen purging (min purity: 99.998 %). A Gamry Reference 600^{TM} potentiostat was again used to perform CV between −0.45 and 0.35 V versus MSE.

3 Results and discussion

The catalytic and electrocatalytic properties of nanoporous metals have received a lot of attention in recent years, not only because of the high surface area and interconnected nanoporosity of these structures (see Fig. 1 as an example), but also because of the potential synergistic effect between the alloying elements, which is particularly true for the nanoporous structures formed on Ag–Au–Pt precursor alloys. By dealloying these ternary alloys, nanoporous metal structures with distinctive characteristics and properties are formed with systematic control of the nanoporous structure, as summarized in Table 1, where NPG was used as a benchmark material.

The thickness of the DL, for the same charge density passed, did not vary significantly in ternary alloys; however, the DL measured in the binary alloy was thinner than in the other alloys. This effect has been previously explained by the authors based on the amount of residual silver that remains buried in the core of the ligaments after dealloying [27]. While dealloying was progressing and silver was removed from the so-called dealloying front, the silver removal from the already formed ligaments continued; however, because platinum reduces gold mobility (i.e., platinum has much lower surface diffusion rate than gold), the initial coarsening of the structure was hindered in the case of ternary alloys, resulting in higher silver contents (in average 48 at% near the surface of the sample as shown in Table 2 and reported elsewhere [27]) and thicker layers than in the case of the Ag–Au alloys (silver content of ca. 29 at% near the surface of the sample—Table 2). In other words, the thinner DL observed in the binary alloy was due to the exposure of buried silver to the electrolyte during coarsening of the structure. The ligament size decreased with the platinum content of the alloy, which is also a consequence of the suppression of the coarsening of the nanoporous structure. As reported in Table 1, the average ligament size for the binary nanostructure was ca. 14 nm, whereas the ligament size for the alloy with 1 at% platinum was ca. 7 nm. By increasing the amount of platinum in the precursor, the size of the ligaments kept decreasing to a value of ca. 4 nm. The roughness factor showed that by reducing the ligament size of the structure, the increase in surface area was substantial. With the decrease in the ligaments size, there was a decrease in the median pore size of the nanostructures: for NPG the pore size was ca. 17 nm, whereas for the structures formed on the alloys with 1, 2, and 3 at% platinum, the pore size was ca. 12, 8, and 6 nm, respectively. These average pore sizes agreed very well with the observations made from TEM images (light regions in Fig. 2 for NPG and for the ternary alloy with the lowest platinum content).

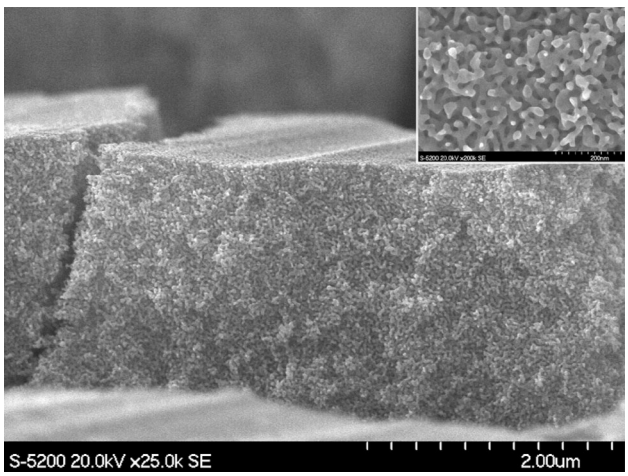

Fig. 1 Interconnected ligament/pore structure formed on the Ag_{77}: Au_{23} alloy after passing 5 C cm^{-2} at 40 °C and 0.55 V versus MSE. The *insert* shows a higher magnification SEM image of the nanoporosity

The surface coverage of platinum in the ternary nanostructures, obtained by hydrogen UPD in 1 M H_2SO_4, is shown in Table 2. As can be seen, the fraction of platinum on the surface of the structures increased from 1.4 to 6.6 % of the real surface area of the nanoporous structures [27]. According with the platinum content of the precursor, and the estimated distance between surface platinum atoms on the ligaments, it is recognized that platinum with few platinum neighbors may not be showing up in the UPD results [47, 48]. Therefore, we recognize that this is an important area for further development, which could be critical for better understanding of the catalytic properties of these nanomaterials. The platinum concentration in the vicinity of the surface of the nanostructures is also shown in Table 2. For the structure formed on the alloy with originally 1 at% platinum, the platinum concentration increased to 3.3 at%, whereas the platinum concentration for the structure with the highest platinum content was 9.1 at%. In all cases, the ratio gold to platinum was nominally

Table 1 Physical characteristics and roughness factors of the nanoporous structures developed at 25 °C and 0.55 V versus MSE in 0.77 M $HClO_4$. Charge density: 5 C cm^{-2}. The number in brackets represents the 95 % confidence interval (CI)

Precursor alloys	Thickness of the DL (μm)[a]	Ligament width (nm)[a]	Pore size (nm)[b]	Roughness factor (R_f)[c]
Ag_{77}:Au_{23}	7.8 (0.2)	13.8 (0.7)	17.2	894 (17)
Ag_{77}:Au_{22}:Pt_1	9.1 (0.9)	6.8 (0.4)	11.6	1941 (238)
Ag_{77}:Au_{21}:Pt_2	9.4 (0.2)	6.0 (0.2)	8.1	2486 (88)
Ag_{77}:Au_{20}:Pt_3	9.7 (0.5)	4.3 (0.2)	5.8	2679 (81)

[a] The 95 % CI was calculated from at least 30 measurements for each quantity

[b] Obtained by BET pore size distribution analysis using the NLDFT method and considering the adsorption branch model

[c] The 95 % CI was calculated from triplicate runs

Table 2 Fraction of platinum atoms on the outermost surface of the ligaments and composition of the DL (silver and platinum) in the vicinity of the surface. All nanoporous structures were developed at 25 °C and 0.55 V versus MSE in 0.77 M $HClO_4$. Charge density: 5 C cm^{-2}. The number in brackets represents the 95 % confidence interval (CI)

Precursor alloys	Fraction of platinum on the surface (%)[a]	Platinum content in the vicinity of the surface (at%)[b]	Retained silver content in the vicinity of the surface (at%)[b]
Ag_{77}:Au_{23}	N/A	N/A	28.8 (4.4)
Ag_{77}:Au_{22}:Pt_1	1.4 (0.7)	3.3 (0.6)	48.9 (2.1)
Ag_{77}:Au_{21}:Pt_2	3.0 (0.9)	5.2 (0.3)	46.7 (0.9)
Ag_{77}:Au_{20}:Pt_3	6.6 (1.0)	9.1 (1.0)	48.1 (3.4)

[a] Obtained by Hydrogen UPD. The 95 % CI was calculated from triplicate runs

[b] Obtained by TEM-EDS analysis. The 95 % CI was obtained from at least three points along the DL

the same as the original alloy, confirming that only silver was removed during dealloying.

Figure 3 shows the CV profiles of all the nanoporous structures in the supporting electrolyte (5 M KOH). A high concentration of KOH was chosen because otherwise there could be some depletion of OH^- at the plane electrode interface coincident with the depletion of methanol—considering that for oxidation of the alcohol to carbonate, $8OH^-$ are consumed for every methanol oxidized. This would be a confusing factor for any analysis of the data, so any such effect was eliminated by having the OH^- concentration at least 10x the methanol concentration. This, together with the higher diffusivity of OH^- compared with methanol, minimizes this effect even if it does not eliminate it completely. As shown in this figure, NPG had an extended double-layer region between −0.9 V and 0.25 V versus Hg/HgO. At 0.25 V, an oxidation peak started, followed by a reduction peak at 0.1 V. These two peaks were ascribed to the formation, and subsequent reduction, of a monolayer of gold surface oxides on the NPG [49]. These observations agreed very well with previous reports for polycrystalline gold [50, 51] and NPG [21]. For the ternary alloys, the oxidation of gold started at a potential 0.1 V less than that of NPG, with the reduction peak also slightly shifted to less positive potential. It was also observed that the magnitude of the reduction peak decreased with increasing platinum content of the alloy. Zhang et al. [21] observed similar trends when characterizing NPG samples with platinum monolayer (s) deposited on the surface of the structure. At ca. −0.5 V, there are reduction peaks that were attributed to the presence of oxidized platinum in the structure. In agreement with Abd El Rehim et al. [52], no influence of silver was detected at this potential after cycling a silver polycrystalline electrode under similar experimental conditions (voltammogram not shown here).

Figure 4a shows the CV profiles for the methanol oxidation reactions of NPG and for the nanostructure formed on the ternary alloy with originally 1 at% platinum. In both cases, the vertical axis corresponds to the nominal current density (i.e., normalized by the geometrical area of the electrode), and the positive scan limit was fixed at 0.2 V to avoid the region in which gold and silver oxides started forming. The ternary nanostructure had higher current

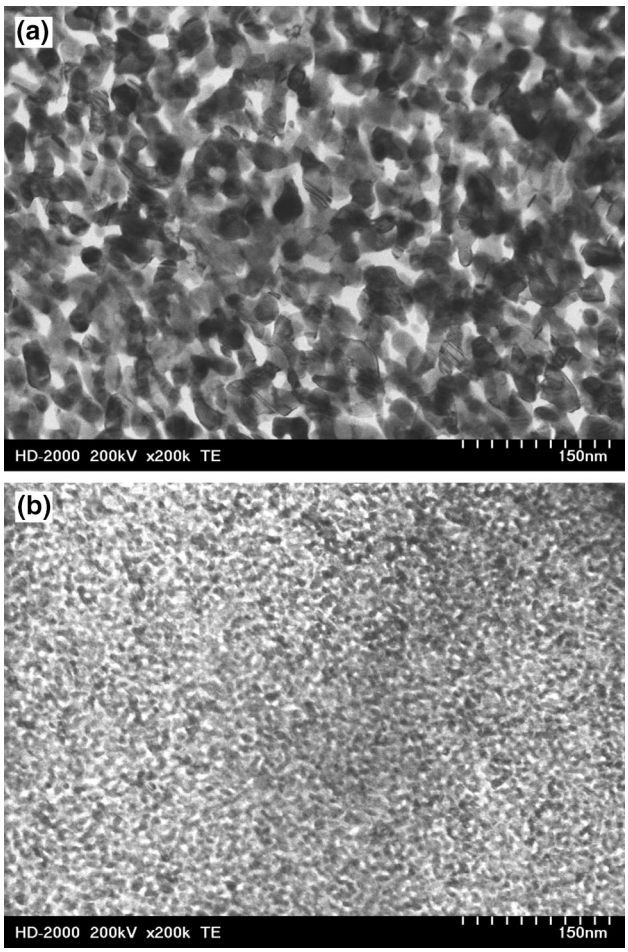

Fig. 2 TEM images of freshly formed nanoporous structures: **a** Ag_{77}:Au_{23}, **b** Ag_{77}:Au_{22}:Pt_1. The dealloying conditions for both alloys were the same—temperature: 25 °C, potential: 0.55 V versus MSE, charged passed: 5 C cm^{-2}

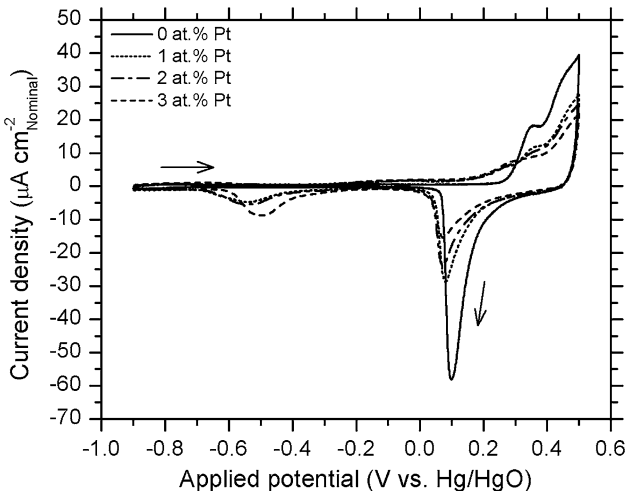

Fig. 3 CV profiles of the different nanoporous structures in 5 M KOH. In all cases, the current density was normalized by the geometrical area of the electrodes. All CV profiles were obtained at 10 mV s^{-1} and 25 °C

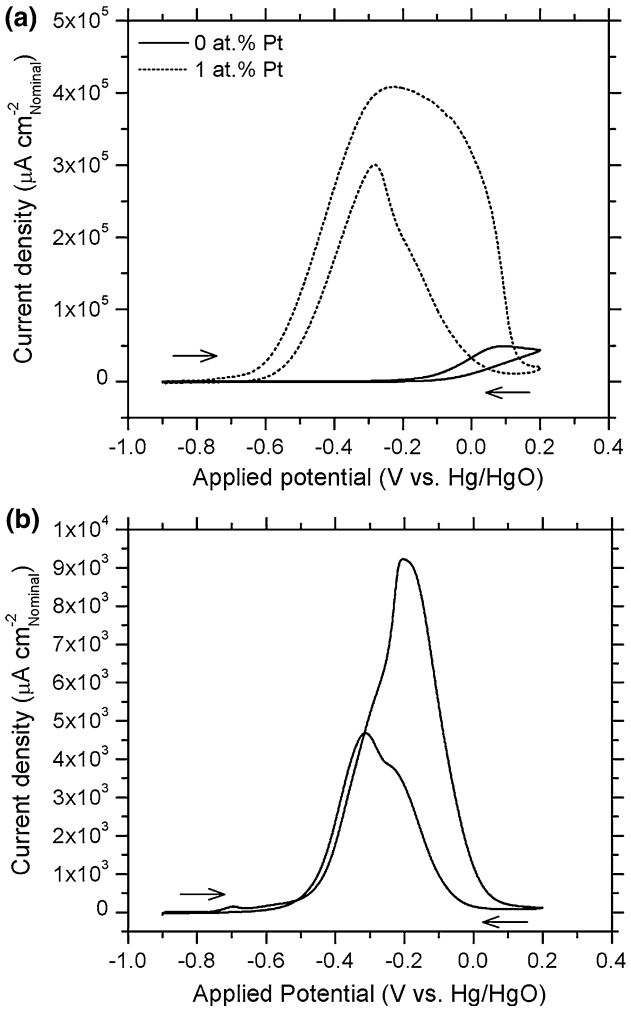

Fig. 4 **a** CV profiles of NPG and the nanoporous structure formed on the alloy with 1 at% platinum; **b** CV profile of polycrystalline platinum. In all cases, the current density was normalized by the geometrical area of the electrodes. All CV profiles were obtained at 10 mV s^{-1} and 25 °C in 5 M KOH–1 M CH_3OH solution

density, with a peak current that was ca. 8 times greater than that in the binary nanostructure. In NPG, the rising current in the forward scan (approximately at −0.2 V) can be ascribed to the characteristic methanol oxidation on the surface (see Fig. 3a for NPG). The pre-oxidation species such as $Au–OH_{ads}^{(1-\lambda)-}$ (λ is the charge transfer coefficient, $0 < \lambda < 1$) are considered by some authors to play a governing role in the electrochemistry of Au in alkaline media; furthermore, the gradual exhaustion of $Au–OH_{ads}^{(1-\lambda)-}$ species is believed to slow down and eventually stop the methanol oxidation reaction (at about 0.15 V vs. Hg/HgO as observed in Fig. 4a) [53]. This potential was very close to the potential at which the gold oxide monolayer started forming. In the case of the ternary alloy, there was a sharp increase in current at more negative potentials than in the binary alloy (approximately at −0.75 V). This

increase in the current density was again related to the characteristic methanol oxidation on the surface (see Fig. 3a for ternary alloys). The peak potential in the forward scan was observed at −0.2 V, whereas another oxidation peak was observed at ca. −0.3 V during the backward sweep. This oxidation peak represents the reaction resuming after the surface of the catalyst was regenerated by dissolving off or reducing any compounds/intermediates that were blocking the structure. A comparison with polycrystalline platinum (Fig. 4b) showed that the oxidation peaks in the forward and backward scans agreed well with those observed in the ternary nanostructure; nevertheless, it is important to emphasize that the nominal current density in the case of the ternary nanostructure was ca. 40 times higher than that for the platinum electrode. A similar behavior was reported by Prabhuram and Manoharan [54] for methanol oxidation with porous platinum electrodes. A comparison with the state-of-the-art Pt–Ru catalyst (e.g., Pt–Ru nanoparticles supported on carbon) and/or with nanoporous platinum constitutes part of the future work with these nanostructures.

Dealloying, by definition, dramatically increases the surface area of the material, which depends, among other things, on the size of the ligaments. As shown in Table 1, the R_f increased by increasing the platinum content of the precursor. Therefore, to account for that effect, the current density was normalized by the true area of the electrode. Following this approach, it was observed that the CV profiles of all ternary nanostructures, under the same experimental conditions, showed a similar trend to the one showed in Fig. 4a. However, it was found that the nanostructure formed on the alloy with 1 at% platinum had slightly higher true methanol oxidation current density than the other two. Figure 5a shows a comparison of the specific activities (taken at −0.35 V vs. Hg/HgO) of the three ternary alloys. It was hypothesized that this result is related to the relative ratio of platinum and gold atoms on the surface of the ligaments. As discussed by Du and coworkers [55] and by Luo and coworkers [56, 57], the synergistic effect between gold and platinum nanoparticles enhances their catalytic activity towards many reactions, including methanol electro-oxidation; however, as suggested elsewhere [28, 55, 58, 59], in alkaline electrolytes, where gold becomes a very active element, there is an *optimum* fraction of platinum atoms surrounded by gold atoms that maximizes the yield of the reaction. Gold atoms are believed to play an important role providing oxygenated species (e.g., adsorption sites for OH^- groups and/or chemisorption of HO_2^- intermediates) in the methanol oxidation process; therefore, this ratio between elements represents a compromise balance of activation of platinum sites and promotion of gold sites by adsorption of OH groups. We are not suggesting, of course, that the nanoporous structure with originally 1 at% platinum,

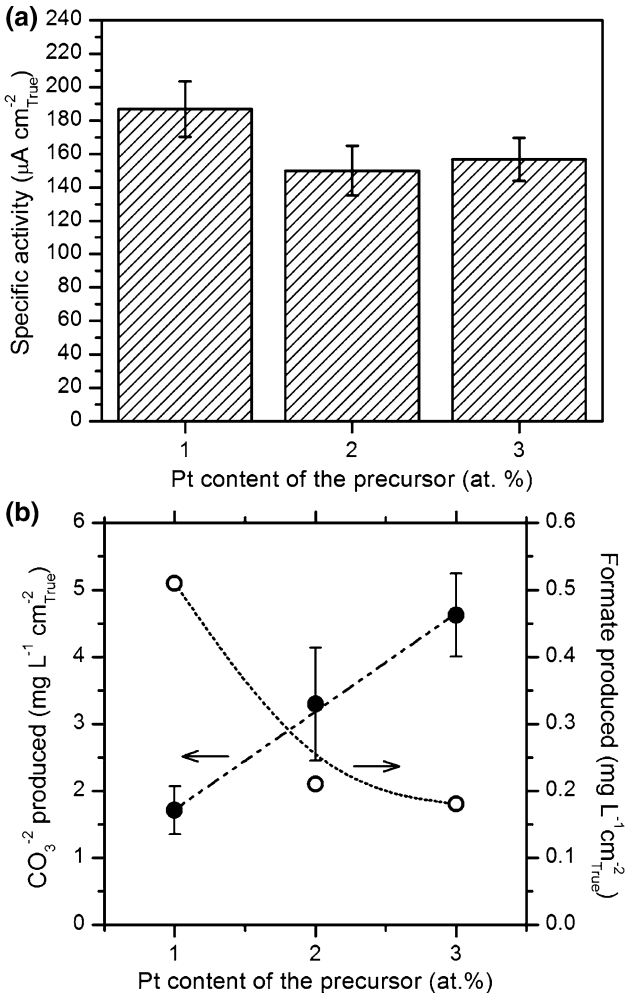

Fig. 5 **a** Summary of specific activities of the ternary alloy structures for the CH_3OH oxidation reaction; the *vertical axis* is the current density per true area of the electrodes. **b** Concentration of carbonate/formate produced after 4000 s of potentiostatic oxidation of CH_3OH. In all cases, the data were obtained at −0.35 V versus Hg/HgO in 5 M KOH–1 M CH_3OH solution; in the case of (**b**), the solution was always agitated with a magnetic stirrer at ca. 700 rpm. The *error bars* represent 95 % CI obtained by triplicate runs

represents that *optimum* composition; however, having most of the platinum atoms surrounded by gold atoms (i.e., platinum being more scattered on the surface), in a highly porous structure, could have a significant role in the observed behavior. Mott and coworkers [28] predicted, by DFT calculations, that a bifunctional electrocatalytic property may be operative in the case of Au–Pt nanoparticles in alkaline electrolyte, where adsorption of CO and OH^- on gold and dehydrogenation of methanol on platinum sites are involved. In acidic electrolytes, on the other hand, the most active structure was the one with higher platinum content (see Sect. 3.2 below).

It has been suggested that among the three likely product of methanol oxidation by gold in alkaline media (i.e.,

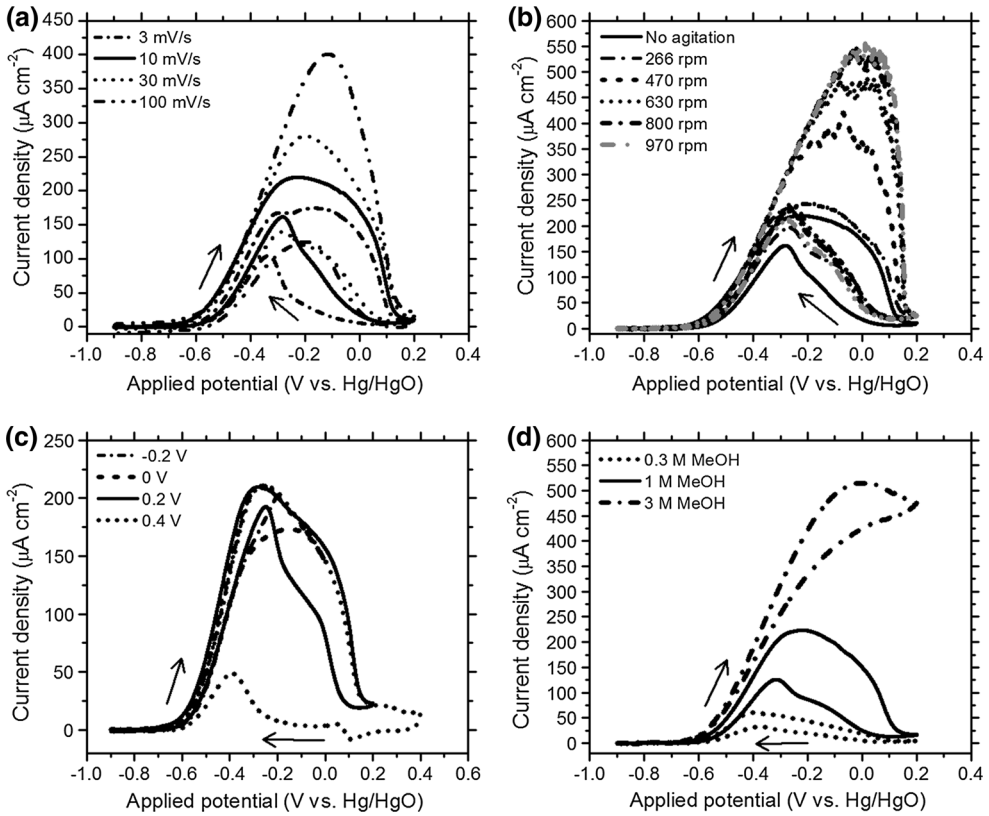

Fig. 6 CV profiles of the nanoporous structures formed on the alloy with 1 at% platinum for the electro-oxidation of CH_3OH in 5 M KOH solution: **a** effect of the scan rates—no external agitation, **b** agitation speeds, **c** scan limit and **d** methanol concentration. For figures **a** to **c**, the methanol concentration was 1 M; for figures **b** to **d**, the scan rate was 10 mV s^{-1}. Temperature: 25 °C. Details about the scan rates, agitation speeds, scan limit, and methanol concentrations are given in figures. In all cases, the current was normalized by the true area of the electrodes

formaldehyde, formate and carbonate), formate is the most probable [50, 53], whereas carbonate tends to be the dominant product when platinum-based catalysts are used [54–60]. To identify the oxidation products formed on the ternary nanoporous metals, potentiostatic experiments at −0.35 V versus Hg/HgO were carried out for at least 4000 s. The fraction of platinum on the surface of the ligaments did not significantly change after these prolonged electrocatalytic experiments; in fact, it was determined that maximum deviation (i.e., reduction) with respect to the as-dealloyed condition was ca. 10 %. NPG was not considered further as ternary alloys were always more catalytic. The quantification of formate by H-NMR is shown in Fig. 5b. The concentration of formate decreased with increasing platinum content of the precursor. No indication of formaldehyde has been found, probably because disproportionation of formaldehyde in highly basic media, according with Cannizzaro's reaction, would occur readily under the current experimental conditions [61]. Carbonate, on the other hand, could be determined by titration with barium solution (1.2 M $BaCl_2$ solution). As shown also in Fig. 5b, the concentration of carbonate produced during the oxidation increased with increasing platinum content of the alloys, which could be a consequence of the higher platinum coverage on the surface of the ligaments. These results suggest that the ratio between the oxidation products could be modified by changing the platinum content of the structure. The low amount of carbonation that occurred during titration was demonstrated by the nearly zero carbonate analysis obtained for the binary alloy (not shown in Fig. 5b).

The effects of different potential scan rates, different agitation speed of the solution (by a magnetic stirrer), different potential scan limits, and methanol concentrations were assessed for all ternary structures. Figure 6 shows the effect of those parameters for the alloy with 1 at% platinum; similar trends were observed for the other ternary alloys. As shown in Fig. 6a, the oxidation current was dependent on the potential scan rate (v); in fact, the peak current was linear with $v^{0.5}$ for all the nanostructures. The oxidation current density associated with the half peak potential (i.e., −0.4 V vs. Hg/HgO) is nearly linear with $v^{0.5}$ for the alloys with 2 and 3 at% platinum, but independent of the scan rate in the case of the lower platinum

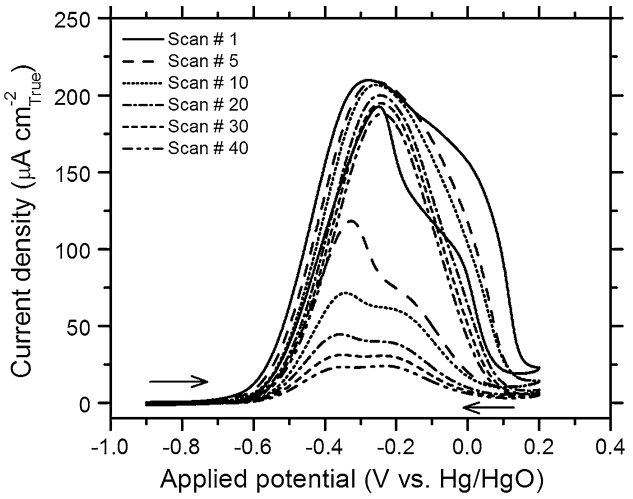

Fig. 7 CV profiles for the electro-oxidation of CH_3OH solution in 5 M KOH on the nanoporous structure formed on the alloy with 1 at% platinum. In all cases, the scan rate was 10 mV s^{-1} and the temperature 25 °C. Details about the number of scan cycles are indicated in figures

content alloy (see Fig. 6a). In the case of the different agitation speeds (i.e., between ca. 200 rpm and 800 rpm), it was observed that the peak current increased with the agitation speed. For example, in the case of the ternary alloy with 1 at% platinum (Fig. 6b), the peak current increased from ca. 200 μA cm^{-2}_{true} (no agitation) to 550 μA cm^{-2}_{true} at 800 rpm (at 970 rpm there were no further changes with respect to 800 rpm). No changes were found in the oxidation current below ca. −0.3 V. Similar trends were observed for the other two ternary alloys (results not shown here). To some extent, the dependence of the peak current density on the scan rate suggests that there is anodic diffusion control (where classically there would be a square root dependence on scan rate), but there are complicating factors including the obvious onset of some kind of inhibition by surface adsorbates. So no secure conclusion can be drawn from the scan rate dependence regarding mass transport control. However, the effect of forced convection shows that there is a natural dependence of peak current density on stirring rate (recognizing that this is not exactly a limiting current density in the usual sense, because of simultaneous complications from adsorption). The saturation of the peak current density at the highest stirring rates is a natural transition from diffusion to activation control under this interpretation, but more detailed study using a formal rotating electrode method would be required to make further progress on that topic.

In terms of the effect of the scan limit (Fig. 6c), it was clear that the oxidation peak in the reverse scan was first observed when the scan limit was 0.2 V; at less positive limits, no oxidation peak was shown, but instead a slight hysteresis was found. This hysteresis could be associated to the blocking of active sites during that stage of the oxidation process. At more positive scan limit (i.e., 0.4 V), two main features were observed in the reverse scan: a smaller oxidation peak at ca. −0.4 V and a cathodic peak at ca. 0.1 V. This cathodic peak was related to the reduction of gold oxide formed on the anodic scan, which also confirmed that gold surface oxide formation occurs at potentials higher than 0.2 V. In terms of the effect of the methanol concentration (Fig. 6d), it was observed that the oxidation current increased linearly with the increasing concentration of methanol; moreover, it was observed that the peak potential moved to less negative potentials while increasing the methanol concentration.

One method to test the electrochemical performance of these nanoporous metals was by repeated potential cycling. Figure 7 shows the effect of different cycles in the ternary structure with originally 1 at% platinum showing a very stable activity toward methanol oxidation, i.e., the specific activity at −0.35 V decreased from 192 μA cm^{-2}_{true} to 130 μA cm^{-2}_{true} after 40 continuous cycles. During the backward sweep, the oxidation peak height was reduced with subsequent scans, which could be associated with small changes in the nanoporous structure. Similar behaviors were observed in the other ternary structures. The binary alloy (not shown here) showed an 80 % reduction in the peak current after 40 cycles.

3.1 Tunability of nanoporous metals and its role in their catalytic response

One of the main advantages of nanoporous metals is that they are highly tunable. By changing the composition of the precursor, the dealloying conditions and/or post-dealloying treatments, changes in the ligament size, the surface composition (i.e., fraction of platinum exposed on the surface of the ligaments), and other characteristics were observed [27]. By exposing the freshly prepared dealloyed ternary structures to laboratory air, at moderately elevated temperature, there is a mixing between the top surface of the ligaments and the layers underneath; during that process, the platinum is pinned on the surface of the structure due to its strong interaction with oxygen allowing us to tune the platinum content of the surface of the ligaments by the *adsorbate-induced surface segregation* mechanism. It is important to mention that before any catalytic test, the electrochemical reduction of any oxidized species on the surface was carried out at ∼−0.3 mV versus MSE in 1 M H_2SO_4 solution. As expected, by exposing the nanostructures to moderate temperature, there is an increase in the atomic surface diffusion, which increases the ligament size in all alloys (see Fig. 8a); for instance, at 425 °C the

ligament size in the structure formed on the alloy with 1 at% platinum increased to 37 nm (right after dealloying the size of the ligaments was ca. 7 nm), whereas the nanostructure with originally 3 at% platinum had the lowest increment in ligament size (from ca. 4 nm to ca. 10 nm). More importantly, however, by exposing the as-dealloyed structures to air at this temperature, the fraction of platinum on the surface of the structures significantly increased (see also Fig. 8a) if compared with the results of as-dealloyed specimens (i.e., minimum platinum coverage) [37].

The change in the platinum content on the surface of the ligaments induced changes in the catalytic response of these nanoporous metals. Figure 8b shows a comparison between the CV profiles of the nanostructures formed on the 1 at% platinum alloy before and after exposure to 425 °C. In both cases, the vertical axis corresponds to the nominal current density. Even after exposure to this moderate temperature, the electrode showed a very high activity, e.g., at −0.35 V the difference in the nominal current density was only 20 % with respect to as-dealloyed samples. However, to account for the effect of surface area, the specific activity at −0.35 V (normalized by the true area of the electrodes) is plotted in Fig. 8c, showing that segregation of platinum induced a very significant increase in the catalytic response of the electrocatalyst. The nanostructure developed on the alloy with 1 at% platinum displayed the highest increment (ca. 400 %) with respect to the as-dealloyed nanostructure. The other nanostructures also showed higher catalytic response after segregation than the as-dealloyed samples, although the activity decreased by increasing the platinum content of the precursor. We could rationalize this finding based on the relative ratio between platinum and gold on the surface of the ligaments and the fact that the supporting electrolyte in the system has high pH (i.e., gold is more active than platinum in basic media). In addition, as previously reported by the authors [37], the structure formed on the alloy with 1 at% platinum showed more traces of silver on the surface than the other two ternary structures. This silver comes from the core of the ligaments after coarsening occurs. Silver could

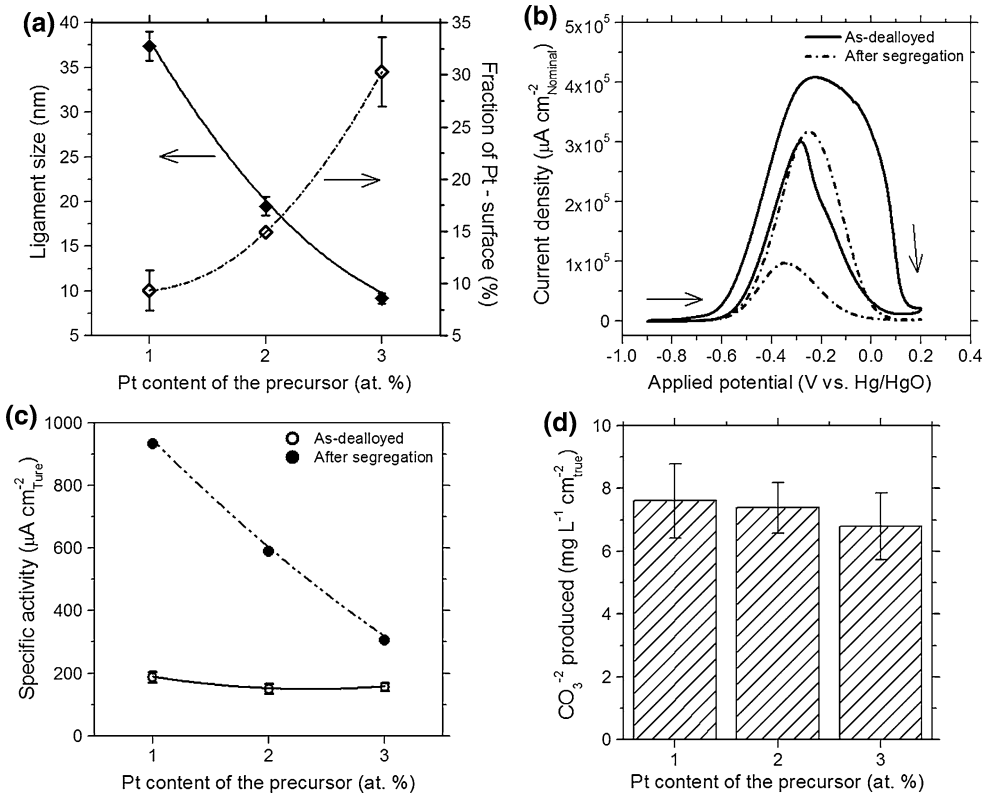

Fig. 8 **a** Ligament size and fraction of platinum on the surface of the ligaments for all ternary structures after exposure to 425 °C for 2 h in the presence of laboratory air; **b** CV profiles in 5 M KOH–1 M CH_3OH solution for the nanoporous structure formed on the alloy with 1 at% platinum structures before and after segregation of platinum, the CV profiles were obtained at 10 mV s^{-1} and 25 °C and the current density was normalized by the geometrical area of the electrodes; **c** Summary of specific activities of the ternary alloy nanostructures for the CH_3OH oxidation reaction at −0.35 V versus Hg/HgO; the *vertical axis* is the current density per true area of the electrodes; **d** concentration of carbonate produced after potentiostatic oxidation at −0.35 V versus Hg/HgO for 400 s; during this time, the solution was agitated with a magnetic stirrer at ca. 700 rpm. The error bars represent 95 % CI obtained by triplicate runs

change the catalytic behavior of the nanostructure by providing additional oxygenated species that interact with methanol species adsorbed on the surface [62, 63].

The concentration of carbonate produced by the nanostructures after platinum segregated to the surface is shown in Fig. 8d. The concentration of carbonate was basically the same for all structures (ca. 7.5 mg L^{-1} cm_{true}^{-2}), which means that for the structure formed on the alloy with 1 at% platinum (i.e., ca. 10 % of the surface atoms were platinum) there was an increase of ca. 300 % with respect to the as-dealloyed structure, whereas for the structure formed on the alloy with 3 at% platinum, an increase of ca. 60 % was observed with respect to the as-dealloyed structure. The current efficiency (considering carbonate as the only product of the oxidation) was 20, 62, and 80 % for the nanostructures with originally 1, 2, and 3 at% platinum, suggesting that other compounds are produced under these experimental conditions (e.g., formate). It is believed that the interaction between gold and platinum surface atoms with the silver atoms exposed to the surface might be responsible for this trend.

Dealloying the ternary alloys at different temperatures also induced changes in the characteristics of the resulting nanostructures, as summarized in Fig. 9. The effect of other dealloying conditions has been previously reported by the authors [27]. By increasing the dealloying temperature, the rate of gold surface diffusion increased, accelerating the coarsening of the ligaments (Fig. 9a). This agreed well with the literature associated with the relaxation of roughened gold surfaces [64–66]. The average ligament width in NPG changed from ca. 14 nm at 25 °C to almost 28 nm at 60 °C. In ternary alloys, a much smaller increase of approximately 10 % was found for the nanostructure with originally 1 at% platinum (from ca. 6.8 nm at 25 °C to 7.4 nm at 60 °C). Variations in the dealloying temperature also induced changes in the depth of the layer (inset in Fig. 9a); in general, the thickness of the layer, for a constant charge density, increased with temperature on the ternary alloys, whereas in the binary alloy, it tended to decrease. These tendencies were related to the fraction of silver retained in the layer (not shown here but discussed elsewhere [27]). Moreover, by increasing the dealloying temperature, the fraction of platinum atoms on the surface of the ligaments increased, as shown in Fig. 9b. By changing the dealloying temperature from 10 to 60 °C, the fractional coverage of platinum atoms increased for all ternary structures, doubling the platinum coverage at the upper temperature. This increase in the platinum coverage on the surface could be associated with the dealloying mechanism itself and/or other processes that were favored under the experimental conditions used here (e.g., preferential adsorption of OH groups on platinum atoms as suggested before for multimetallic nanoparticles [67]).

Figure 9c shows the specific activity (taken from cyclic voltammograms at −0.40 V vs. Hg/HgO—not shown here)

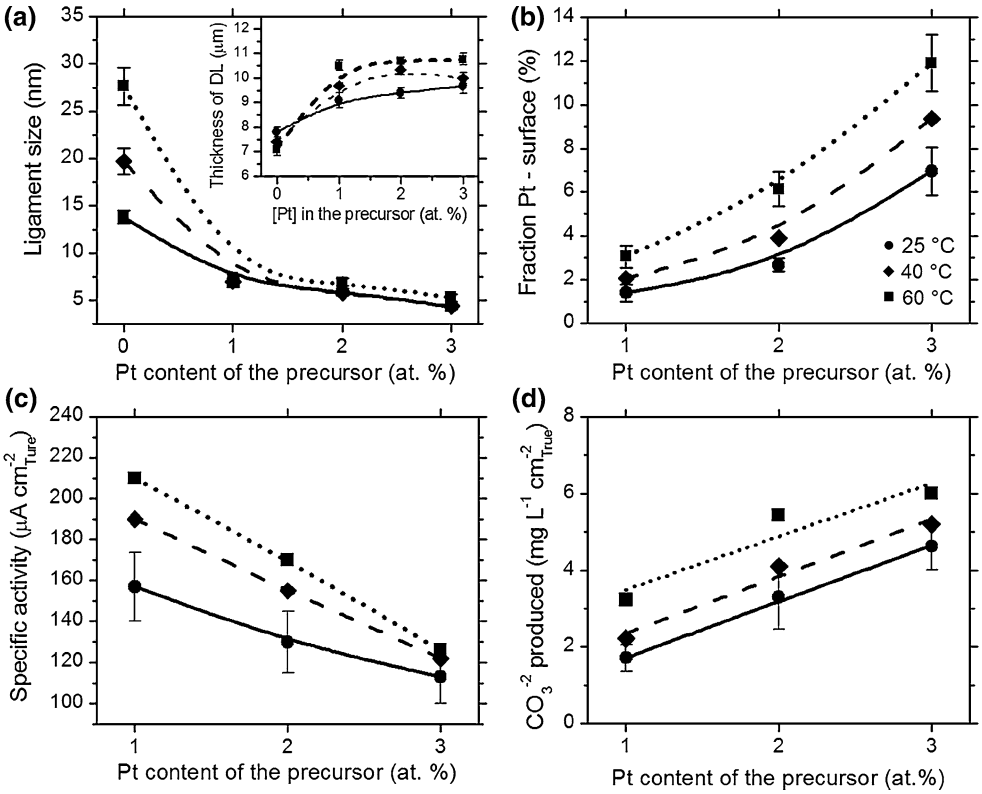

Fig. 9 Effect of the dealloying temperature on the main characteristics and catalytic activity of the resulting nanoporous structures: **a** effect on the size of the ligaments; the *insert* in this figure shows the average thickness of the DL; **b** fraction of platinum on the surface of the ligaments; **c** summary of specific activities toward CH_3OH oxidation at −0.40 V versus Hg/HgO; **d** concentration of carbonate after running the reaction potentiostatically at −0.40 V versus Hg/HgO for 4000 s. Details about the different dealloying temperatures are indicated in figure (**b**). The *error bars* represent 95 % CI obtained by triplicate runs

for the three ternary nanostructures developed under different dealloying temperatures. The catalytic responses of structures developed at other dealloying conditions (e.g., dealloying time) have been tested but not reported here. By increasing the temperature of the electrolyte (for a constant dealloying charge density), the specific activity of the nanostructures increased, which is rationalized by the change in the surface composition of the ligaments (i.e., higher platinum coverage). The concentration of carbonate in solution (see Fig. 9d) also increased by increasing the dealloying temperature. The current efficiency for the ternary nanostructures developed at 60 °C was 85, 93, and 98 % for the alloys with 1, 2, and 3 at% platinum respectively. Once again, for this analysis, carbonate is considered the only product of the oxidation.

3.2 Methanol electro-oxidation in acidic media

To better understand the electrocatalytic properties of these novel nanoporous metals, a preliminary assessment of their catalytic response in an acidic electrolyte has been performed. Figure 10a shows the CV profiles of all the nanoporous structures in 0.5 M $HClO_4$. As for the basic solutions, the concentration of the supporting electrolyte was also experimentally determined choosing the concentration at which the highest current density was observed (results not shown here). As can be seen in this figure, the double-layer region in NPG extended from −0.45 to 0.10 V versus MSE. At 0.10 V, an increase in the current density was observed, which could be associated with the beginning of the oxidation of gold. No reduction peaks were observed in the range of potentials under investigation. At higher scan limits, an oxidation peak, with the subsequent reduction peak, were associated with gold. For the ternary alloys, reversible waves caused by hydrogen adsorption/desorption at potentials lower than 0.3 V were observed. An increase in the oxidation current was detected for all ternary alloys at potentials higher than 0.10 V, with the alloy with 3 at% platinum showing the increase in current density at slightly more negative potentials than the other two ternary alloys. A characteristic reduction peak around 0 V was associated with the reduction of platinum oxides that were formed during the anodic scan [54, 68].

Figure 10b shows the CV profiles for the methanol oxidation reactions of all nanostructures in acid. The positive scan limit was fixed at 0.35 V to minimize the impact of surface oxides and evaluate the catalytic response of these nanostructures mostly in a region below the empirical critical potential of these alloys (i.e., ca. 0.35 V in 0.77 M $HClO_4$) [27]; nevertheless, better understanding of the impact of further dealloying under these experimental conditions is part of our future effort. In NPG, there was basically no catalytic response in this region of potentials;

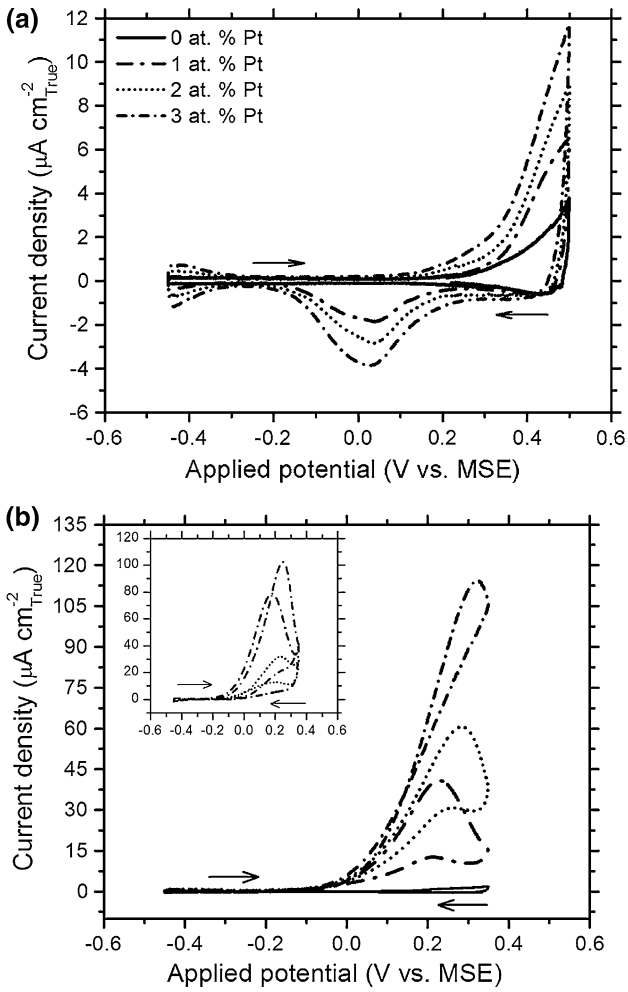

Fig. 10 **a** CV profiles of the different nanoporous structures in 0.5 M $HClO_4$; **b** CV profiles of the nanoporous structures in 0.5 M $HClO_4$–1 M CH_3OH solution. The *insert* in **b** corresponds to the CV profiles in 0.5 M $HClO_4$–1 M CH_3OH solution after segregation of platinum at 425 °C in laboratory air for 2 h. The original platinum composition is shown in **a**. All CV profiles were obtained at 10 mV s^{-1}. The temperature in all cases was 25 °C

at higher potentials, however, it has been reported that gold becomes a relatively active catalyst for methanol oxidation [50]. In the case of the ternary alloys, there was an obvious increase in current at −0.10 V; this increase in the true current density was related to the characteristic methanol oxidation on the surface (see Fig. 10a). The peak potential in the case of the nanostructure formed on the alloy with 1 at% platinum was located at ca. 0.23 V, whereas in the case of the nanostructure formed on the 3 at% platinum alloy, the peak potential shifted to more positive potential (ca. 0.32 V). The peak current was ca. 2.5 times higher in the 3 at% platinum alloy than in the 1 at% platinum. In contrast with the results obtained in alkaline electrolyte, the highest platinum content nanostructure was the most active catalyst; nevertheless, it was

clear that these nanostructures displayed higher electrocatalytic response in alkaline media. This result agreed well with the observations made on supported gold–platinum nanoparticles when evaluated as electrocatalysts for methanol oxidation in acidic electrolyte, where high contents of platinum were required to maximize the activity of the catalyst [28, 58, 59].

As was reported before, by exposing the as-dealloyed structures to 425 °C in the presence of air, there was a clear tendency of platinum to segregate to the surface of the ligaments; therefore, it was an obvious step to analyze the catalytic response of these tuned structures toward methanol oxidation in $HClO_4$ supporting electrolyte. The inset in Fig. 10b shows the CV profiles of all ternary structures in a solution containing methanol. As can be seen, the structure formed on Ag_{77}:Au_{20}:Pt_3 displayed higher specific activity than that in the as-dealloyed sample (e.g., at 0.2 V, the true current density in the as-annealed sample was 40 % higher than that in the as-dealloyed electrode). The peak current, on the other hand, slightly decreased with the heat treatment. In the backward scan, the sample after segregation had a well-defined oxidation peak, which was not clearly observed in the sample before the heat treatment. Increasing the fraction of platinum on the surface from ca. 6 to ca. 30 % did improve the electrocatalytic response of the nanostructure, even though the surface area slightly decreases (i.e., ligament size increased). In the other two nanostructures (formed on Ag_{77}:Au_{22}:Pt_1 and Ag_{77}:Au_{21}:Pt_2 alloys), a decrease in the electrocatalytic activity was observed, with the bigger decay in the one formed on the alloy with 1 at% platinum.

4 Conclusions

(a) Novel nanoporous structures have been formed by electrochemically removing silver from Ag–Au–Pt alloys with platinum contents of 1, 2, and 3 at%. In these structures, the surface is mostly covered by the more-noble elements (i.e., gold and platinum) through the whole thickness of the DL.

(b) The characteristics of the resulting nanoporous metals depend on the platinum content of the precursor. By increasing the platinum concentration, the ligament size decreases and the platinum coverage on the surface of the ligaments increases. Moreover, by having gold and platinum on the surface of the nanostructure, the catalytic response toward methanol oxidation is significantly enhanced showing an onset of the reaction at more negative potentials, higher current densities, longer stability, and electrocatalytic activity.

(c) Based on the original platinum content of the ternary alloy precursors, and the estimated distance between platinum atoms in the nanoporous material, it is believed that the fraction of platinum obtained by UPD of hydrogen represents the minimum platinum coverage of the ligaments. This clearly becomes an important area for further development to better understand the catalytic properties of these and other nanomaterials.

(d) Among all the three ternary nanostructures, the one developed on the alloy with 1 at% platinum shows the highest activity toward methanol electro-oxidation in alkaline electrolyte. Gold and platinum clearly display a remarkable synergistic effect; however, the ratio gold to platinum seems to play an important role in alkaline electrolytes.

(e) In alkaline media, formate and carbonate were identified as the main products of the oxidation reaction. In the case of NPG, mostly formate was detected (the amount of carbonate formed during the reaction was minimal), whereas a combination of the two products was detected when the ternary nanostructures were used. More importantly, by increasing the platinum content of the ternary precursor, the ratio of the reaction products can be modified.

(f) By forming nanoporous metals at different dealloying temperatures, the characteristics of the resulting structures change (e.g., platinum coverage on the surface and ligament size). Moreover, the catalytic performance toward methanol oxidation also changes showing that the specific activity of all nanostructures increases with the dealloying temperature. The concentration of carbonate produced increases also with the dealloying temperature.

(g) By inducing segregation of platinum to the surface of the ligaments (after exposure to 425 °C in the presence of air), there is a significant increase in the current density in all ternary structures in alkaline media, especially in the one formed on the alloy with 1 at% platinum.

(h) In the presence of an acidic electrolyte ($HClO_4$), the structure with the highest platinum content is the one showing the highest specific activity toward methanol electro-oxidation (ca. 110 μA cm^{-2}_{true} at 0.3 V vs. MSE). The effect of segregating platinum to the surface of the ligaments also induces an increase in the current density in all structures.

Acknowledgments The authors wish to thank D. Burns and J. A. Tang, from the Nuclear Magnetic Resonance Facility at the Department of Chemistry—University of Toronto, for their help in the performance of the NMR experiments. The authors wish also to acknowledge the financial support from the Natural Sciences and Engineering Research Council (NSERC) of Canada.

References

1. Haruta M, Kobayashi T, Sano H, Yamada N (1987) Novel gold catalyst for the oxidation of carbon monoxide at a temperature far below 0 °C. Chem Lett 16:405–408
2. Bond JC, Louis C, Thompson DT (2006) Catalysis by gold. Imperial College Press, London
3. Meyer R, Lemire C, Shaikhutdinov ShK, Freund HJ (2004) Surface chemistry of catalysis gold. Gold Bull 37:72–124
4. Dimitratos N, Lopez-Sanchez JA, Morgan D, Carley A, Prati L, Hutchings GJ (2007) Solvent free liquid phase oxidation of benzyl alcohol using Au supported catalyst prepared using a sol immobilization technique. Catal Today 122:317–324
5. Della Pina C, Falletta E, Rossi M (2008) Highly selective oxidation of benzyl alcohol to benzaldehyde catalyzed by bimetallic gold-copper catalyst. J Catal 260:384–386
6. Abd El-Moemen A, Kučerová G, Behm RJ (2010) Influence of H_2, CO_2 and H_2O on the activity and deactivation behavior of Au/CeO_2 catalysts in the water gas shift reaction at 300°C. Appl Catal B 95:57–70
7. Dimitratos N, Prati L (2005) Gold based bimetallic catalyst for liquid phase applications. Gold Bull 38:73–77
8. McPherson JS, Thompson DT (2009) Selectivity of gold catalyst for applications of commercial interest. Top Catal 52:743–750
9. Corma A, Garcia H (2008) Supported gold nanoparticles as catalysts for organic reactions. Chem Soc Rev 37:2096–2126
10. Moulijn JA, van Diepen AE, Kapteijn F (2001) Catalyst deactivation: is it predictable? What to do? Appl Catal A 212:3–16
11. Campbell CT, Parker SC, Starr DE (2002) The effect of size dependent nanoparticle energetics on catalyst sintering. Science 298:811–814
12. Koga K, Ikeshoji T, Sugawara K (2004) Size and temperature-dependent structural transition in gold nanoparticles. Phys Rev Lett 92:115507
13. Yeh YC, Creran B, Rotello VM (2012) Gold nanoparticles: preparation, properties and applications in bionanotechnology. Nanoscale 4:1871–1880
14. Daniel MC, Astruc D (2004) Gold nanoparticles: assembly, supramolecular chemistry, quantum-size-related properties, and applications towards biology, catalysis, and nanotechnology. Chem Rev 104:293–346
15. Haruta M (2002) Catalysis of gold nanoparticles deposited on metal oxides. Cattech 6:102–115
16. Schubert MM, Hackenberg S, van Veen AC, Muhler M, Plzak V, Behm RJ (2001) CO oxidation over supported gold catalysts-"inert" and "active" support materials and their role for the oxygen supply during reaction. J Catal 197:113–122
17. Comotti M, Li WC, Spliethoff B, Schuth F (2006) Support effect in high activity gold catalysts for CO oxidation. J Am Chem Soc 128:917–924
18. Fujita T, Guan PF, McKenna K, Lang XY, Hirata A, Zhang L, Tokunaga T, Arai S, Yamamoto Y, Tanaka N, Ishikawa Y, Asao N, Yamamoto Y, Erlebacher J, Chen MW (2012) Atomic origins of the high catalytic activity of nanoporous gold. Nat Mater 11:775–780
19. Biener J, Wittstock A, Baumann TF, Weissmüller J, Bäumer M, Hamza AV (2009) Surface chemistry in nanoscale material. Materials 2:2404–2428
20. Haruta M (2007) New generation of gold catalysts: nanoporous foams and tubes—is unsupported gold catalytically active? Chem Phys Chem 8:1911–1913
21. Zhang J, Liu P, Ma H, Ding Y (2007) Nanostructured porous gold for methanol electro-oxidation. J Phys Chem C 111: 10382–10388
22. Erlebacher J (2004) An atomistic description of dealloying: porosity evolution, the critical potential, and rate-limiting behaviour. J Electrochem Soc 151:C614–C626
23. Ding Y, Chen M, Erlebacher J (2004) Metallic mesoporous nanocomposites for electrocatalysis. J Am Chem Soc 126:6876–6877
24. Ge X, Wang R, Liu P, Ding Y (2007) Platinum-decorated nanoporous gold leaf for methanol electrooxidation. Chem Mater 19:5827–5829
25. Zeis R, Mathur A, Fritz G, Lee J, Erlebacher J (2007) Platinum plated nanoporous gold: an efficient, low Pt loading electrocatalyst for PEM fuel cells. J Power Sources 165:65–72
26. Snyder J, Asanithi P, Dalton AB, Erlebacher J (2008) Stabilized nanoporous metals by dealloying ternary alloy precursors. Adv Mater 20:4883–4886
27. Vega AA, Newman RC (2014) Nanoporous metals fabricated through electrochemical dealloying of Ag–Au–Pt with systematic variation of Au: Pt ratio. J Electrochem Soc 161:C1–C10
28. Mott D, Luo J, Njoki PN, Lin Y, Wang L, Zhong CJ (2007) Synergistic activity of gold-platinum alloy nanoparticle catalysts. Catal Today 122:378–385
29. Zhao D, Xu B (2006) Enhancement of Pt utilization in electrocatalysts by using gold nanoparticles. Angew Chem Int Ed 45:4955–4959
30. Stamenkovic VR, Mun BS, Arenz M, Mayrhofer KJJ, Lucas CA, Wang GF, Ross PN, Markovic NM (2007) Trends in electrocatalysis on extended and nanoscale Pt-bimetallic alloys surfaces. Nat Mater 6:241–247
31. Gohda Y, Groß A (2007) Structure-reactivity for bimetallic electrodes: Pt overlayers and PtAu surface alloys on Au (111). J Electroanal Chem 607:47–53
32. Wolter SD, Brown B, Parker CB, Stoner BR, Glass TJ (2010) The effect of gold on platinum oxidation in homogeneous Au-Pt electrocatalysts. Appl Surf Sci 257:1431–1436
33. Brown B, Wolter SD, Stoner BR, Glass JT (2008) Alloying effects of co-sputtered gold-platinum thin films on the oxygen reduction reaction in acidic electrolyte. J Electrochem Soc 155:B852–B859
34. Schwank J (1985) Gold in bimetallic catalysts. Gold Bull 18:2–10
35. Pedersen MØ, Helveg S, Ruban A, Stensgaard I, Lægsgaard E, Nørskov JK, Besenbacher F (1999) How a gold substrate can increase the reactivity of a Pt overlayer. Surf Sci 426:395–409
36. Zhang J, Ma H, Zhang D, Liu P, Tian F, Ding Y (2008) Electrocatalytic activity of bimetallic platinum-gold catalysts fabricated based on nanoporous gold. Phys Chem Chem Phys 10:3250–3255
37. Vega AA, Newman RC (2014) Beneficial effects of adsorbate-induced surface segregation of Pt in nanoporous metals fabricated by dealloying of Ag-Au-Pt alloys. J Electrochem Soc 161:C11–C19
38. Waszczuk P, Zelenay P, Sobkowski J (1995) Surface interaction of benzoic acid with a copper electrode. Electrochim Acta 40:1717–1721
39. Kuźmierczyk K, Łukaszewski M, Siwek SRZH, Kotowski J, Czerwiński A (2002) Electrochemical behaviour of Pt-Au alloys. Pol J Chem 76:607–618
40. Trasatti S, Petrii OA (1992) Real surface area measurements in electrochemistry. J Electroanal Chem 327:353–376
41. Hayes M, Kuhn AT (1980) Determination of platinum catalyst surface area with potentiodynamic techniques—effect of experimental parameters. Appl Surf Sci 6:1–14
42. Biegler T, Rand DAJ, Woods R (1971) Limiting oxygen coverage on platinized platinum: relevance to determination of real platinum area by hydrogen adsorption. J Electroanal Chem Interfacial Electrochem 29:269–277
43. Doña-Rodríguez JM, Herrera-Melián JA, Pérez-Peña J (2000) Determination of the real surface area of Pt electrodes by

hydrogen adsorption using cyclic voltammetry. J Chem Educ 77:1195
44. Chen PC (1999) Precipitation of barium carbonate in a pH-STAT semi-batch crystallizer. 14th international symposium on industrial crystallization. Institution of Chemical Engineers, Cambridge, pp 9–14
45. Kubota N, Sekimoto T, Shimizu K (1990) Precipitation of $BaCO_3$ in a semi-batch reactor with double-tube gas injection nozzle. J Cryst Growth 102:434–440
46. Teicher H (1955) Precipitation of barium carbonate. Anal Chem 27:1416–1418
47. Bergbreiter A, Alves OB, Hoster HE (2010) Entropy effects in atom distribution and electrochemical properties of Au(x)Pt(1 − x)/Pt(111) surface alloys. Chem Phys Chem 11:1505–1512
48. Moroun F, Ozanam F, Magnussen OM, Behm RJ (2001) The role of atomic assembles in the reactivity of bimetallic electrocatalysts. Science 293:1811–1814
49. Pourbaix M (1974) Atlas of Electrochemical equilibria in aquous solutions. NACE International, Houston
50. Borkowska Z, Tymosiak-Zielinska A, Shul G (2004) Electrooxidation of methanol on polycrystalline and single crystal gold electrodes. Electrochim Acta 49:1209–1220
51. Hernández J, Solla-Gullón J, Herrero E, Aldaz A, Feliu JM (2006) Methanol oxidation on gold nanoparticles in alkaline media: unusual electrocatalytic activity. Electrochim Acta 52:1609–1662
52. Abd El Rehim SS, Hassam HH, Ibrahim MAM, Amin MA (1998) Electrochemical behaviour of a silver electrode in NaOH solutions. Monatshefte fur Chemie 129:1103–1117
53. Assiongbon KA, Roy D (2005) Electro-oxidation of methanol on gold in alkaline media: adsorption characteristics of reaction intermediates studied using time resolved electro-chemical impedance and surface plasmon resonance techniques. Surf Sci 594:99–119
54. Prabhuram J, Manoharan R (1998) Investigation of methanol oxidation on unsupported platinum electrodes in strong alkali and strong acid. J Power Sources 74:54–61
55. Du Y, Xu JJ, Chen HY (2009) Ultrathin platinum film covered high-surface-area nanoporous gold for methanol electrooxidation. Electrochem Commun 11:1717–1720
56. Lou Y, Maye MM, Han L, Luo J, Zhong CJ (2001) Gold-platinum alloy nanoparticles assembly as catalyst for methanol electrooxidation. Chem Commun 154:473–474
57. Luo J, Maye MM, Kariuki NN, Wang L, Njoki P, Lin Y, Schadt M, Naslund HR, Zhong CJ (2005) Electrocatalytic oxidation of methanol: carbon-supported gold-platinum nanoparticle catalysts prepared by two phase protocol. Catal Today 99:291–297
58. Wanjala BN, Luo J, Fang B, Mott D, Zhong CJ (2011) Gold-platinum nanoparticles: alloying and phase segregation. J Mater Chem 21:4012–4020
59. Zhong CJ, Luo J, Njoki PN, Mott D, Wanjala B, Loukrakpam R, Lim S, Wang L, Fang B, Xu ZC (2008) Fuel cell technology: nano-engineered multimetallic catalysts. Energy Environ Sci 1:454–466
60. Hao-Yu E, Scott K, Reeve RW (2003) A study of the anodic oxidation of methanol on Pt in alkaline solutions. J Electroanal Chem 547:17–24
61. Geissman TA (2011) The cannizzaro reaction. Organic reactions. Wiley, New York, pp 94–113
62. Wittstock A, Neumann B, Schaefer A, Dumbuya K, Kübel C, Biener MM, Zielasek V, Steinrück HP, Gottfried JM, Biener J, Hamza A, Baümer M (2009) Nanoporous Au: an unsupported pure gold catalyst? J Phys Chem C 113:5593–5600
63. Wittstock A, Zielasek V, Biener J, Friend CM, Bäumer M (2010) Nanoporous gold catalysts for selective gas-phase oxidative coupling of methanol at low temperature. Science 327:319–322
64. Andreasen G, Nazzarro M, Ramirez J, Salvarezza RC, Arvia AJ (1996) Kinetics of particles coarsening at gold electrode/electrolyte solution interfaces followed by in situ scanning tunneling microscopy. J Electrochem Soc 143:466–471
65. Doña JM, González-Velasco J (1993) Mechanism of surface diffusion of gold adatoms in contact with an electrolytic solution. J Phys Chem 97:4714–4719
66. García MP, Gómez MM, Salvarezza RC, Arvia AJ (1993) Effect of the solution composition and the applied potential on the kinetics of roughness relaxation at gold electrodes in slightly acid electrolytes. J Electroanal Chem 347:237–246
67. Wang C, van der Vliet D, More KL, Zaluzec NJ, Peng S, Sun SH, Daimon H, Wang GF, Greeley J, Pearson J, Paulikas AP, Karapetrov G, Strmcnik D, Markovic NM, Stamenkovic VR (2011) Multimetallic Au/FePt3 nanoparticles as highly durable electrocatalyst. Nano Lett 11:919–926
68. Tripkovic AV, Gojkovic SL, Popovic KD, Lovic JD (2006) Methanol oxidation at platinum electrodes in acid solution: comparison between model and real catalysts. J Serb Chem Soc 71:1333–1343